# X-ray method to study temperature-dependent stripe domains in MnAs/GaAs(001)

R. Magalhães-Paniago[a,b], L.N. Coelho[a], B.R.A. Neves[a],
H. Westfahl Jr.[b], F. Iikawa[c], L. Däweritz[d], C. Spezzani[e], and M. Sacchi[e]
[a]*Departamento de Física, Universidade Federal de Minas Gerais, CP 702, Belo Horizonte MG, 30123-970 Brazil.*
[b]*Laboratório Nacional de Luz Síncrotron, CP 6192, Campinas SP, 13084-971, Brazil.*
[c]*Instituto de Física "Gleb Wataghin", UNICAMP, CP 6165, 13083-970 SP, Brazil.*
[d]*Paul-Drude-Institut für Festkörperelektronik, Hausvogteiplatz 5-7, 10117 Berlin, Germany.*
[e]*Laboratoire pour l'Utilisation du Rayonnement Electromagnétique,*
*Centre Universitaire Paris-Sud, Boîte Postale 34, 91898 Orsay, France.*

MnAs films grown on GaAs (001) exhibit a progressive transition between hexagonal (ferromagnetic) and orthorhombic (paramagnetic) phases at wide temperature range instead of abrupt transition during the first-order phase transition. The coexistence of two phases is favored by the anisotropic strain arising from the constraint on the MnAs films imposed by the substrate. This phase coexistence occurs in ordered arrangement alternating periodic terrace steps. We present here a method to study the surface morphology throughout this transition by means of specular and diffuse scattering of soft x-rays, tuning the photon energy at the Mn 2p resonance. The results show the long-range arrangement of the periodic stripe-like structure during the phase coexistence and its period remains constant, in agreement with previous results using other techniques.

The integration of magnetic films in semiconductor devices represents one of the major challenges in materials science. MnAs is a very promising material for spin injection, in combination with III-V semiconductor compounds (such as GaAs)[1,2]. Around room temperature (RT), bulk MnAs undergoes a first order structural and magnetic phase transition[3,4,5] between the low temperature $\alpha$ phase, hexagonal and ferromagnetic, and the high temperature $\beta$ phase, orthorhombic and paramagnetic. MnAs films grown on GaAs(001)[6,7,8] exhibit a phase coexistence over a temperature range that can extend between 0 °C and 55 °C, depending on the thickness of the film[9,10,11,12]. Several local probe techniques have been used to characterize the surface morphology and magnetic structure, such as atomic force microscopy (AFM)[12], magnetic force microscopy (MFM)[13] and X-ray magnetic circular dichroism photo-emission electron microscopy (XMCDPEEM)[14]. They highlighted the formation of periodic terraces and magnetic domains at intermediate temperatures for the phase transition. Information on the long range order of terraces is usually gained through scattering experiments. In the case of MnAs, x-ray diffraction experiments showed the coexistence of the two crystallographic phases[9,11], but could not address the formation of periodic domains with long range order.

In this work we have used specular and diffuse x-ray reflectivity to follow the formation and evolution with temperature of the terrace morphology throughout the $\alpha-\beta$ phase transition. In contrast to the microscopy technique, such as atomic force microscopy, which probes small area and only near the surface, the x-ray reflectivity technique proposed here analyzes over a much larger area of the surface and deepness, providing long range order information and also the interface. On MnAs films analyzed using this technique we observe the formation and disappearance of diffuse satellite peaks associated with the terrace periodicity as a function of temperature. The modeling of their intensity profiles yields numbers for the temperature-dependent terrace widths.

A 130 nm thick MnAs was grown by molecular beam epitaxy on a GaAs(001) substrate at 250 °C in a growth condition to obtain A-type orientation[8], i.e., the MnAs plane in the $\alpha$ phase parallel to the GaAs $(001)$ plane with the MnAs $[0001]$ c-axis along the GaAs direction.

We have first used AFM to identify the terrace-like steps discussed before. Figure1a depicts a room temperature AFM image of the surface topography of the MnAs film, which shows the formation of stripe-like domains, elongated along the $(0001)$ direction, during the coexistence of two phases and a clear alternate periodic structure between $\alpha$ and $\beta$ phases is observed. Over the extension of the AFM image, these terrace steps appear periodic, with a modulation period of about 600 nm. The lower terraces correspond to regions where no magnetic signal is obtained with Magnetic Force Microscopy (MFM), therefore they can be associated to the high temperature paramagnetic $\beta$ phase. The higher terraces (ferromagnetic $\alpha$ phase) exhibit a complex magnetic structure where domains of opposite orientation seem to be intercalated[13,14]. Several authors have already addressed the magnetic domain structure of these films using MFM techniques, and at least three different types of domain formations were observed[13,14]. Here we will concentrate on our X-ray method to study the terrace configuration.

In order to quantitatively evaluate the surface morphology of the sample, we performed resonant x-ray scattering measurements at beamline SU-7 of the SuperACO storage ring (LURE laboratory, Orsay). The beamline, equipped with a linear undulator source, covers the 100-1000 eV range with a resolving power of about 2000. The endstation is a 2-circle ($\omega/2\theta$) reflectometer working in ultra-high vacuum[15]. As shown in Fig.1b, the scattering geometry was co-planar, with the incoming beam (of wave vector $\mathbf{k}_i$) impinging on 0.5mm x 0.5mm of the MnAs film at a grazing angle , and the scattered photons ($\mathbf{k}_f$) collected at an angle $2\theta$ with respect to the incident beam. The scattering vector $\mathbf{q}=\mathbf{k}_f-\mathbf{k}_i$ can be separated into two components, one parallel $q_x=\frac{2\pi}{\lambda}\left[\cos(2\theta-\omega)-\cos(\omega)\right]$ and one perpendicular $q_z=\frac{2\pi}{\lambda}\left[\sin(2\theta-\omega)+\sin(\omega)\right]$ to the sample surface. A structure that is periodic with a modulation period $\ell$ will give

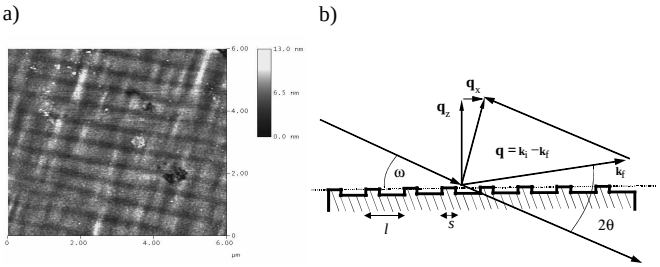


Figure 1: a) Atomic force microscopy image of the 130 nm thick MnAs film grown on GaAs(001); b) Scattering geometry used to examine the terrace step structure. Scattering vectors are described in the text.

rise to constructive interference in the scattering process when $q = \frac{2\pi}{\ell}$.

The horizontal terrace step structure can be studied in detail by performing rocking scans of the sample, i.e. ω scans at fixed 2θ. Over a limited range in ω around specular ($\omega = \frac{2\theta}{2}$), a rocking scan corresponds to a $q_x$ scan at fixed $q_z$. In Fig. 2a we show the map of the scattered intensity that results from a series of 66 $q_x$ scans (201 points each) performed as a function of temperature at a given $q_z$ value (1.68 nm-1, corresponding to $2\theta = 30^\circ$ and photon energy (640 eV). Fig. 2b shows the line plots of three of these scans, at temperatures corresponding to the $\alpha - \beta$ phase coexistence region. In the intermediate temperature region, we observe, besides the specular peak (zero order) at $q_x = 0$, two other peaks (first order) at $q_x = \pm 0.0107\, nm^{-1}$. We ascribe them to the long range lateral order produced by the stripe domains in the phase coexistence temperature region. The associated modulation period is $\ell = \frac{2\pi}{q_x} = 587\, nm$. It is worth noticing that, while the intensity of the first order peaks varies drastically as a function of temperature, their position remains unaltered. This implies that the modulation period of the stripes, i.e. the sum of the widths of the two domains with different structures, remains constant. The α to β transition takes place versus temperature with the widths of the β stripe increasing at the expense of the width of the α phase, their sum remaining constant. This has been previously observed by AFM[12] and by XMCDPEEM[14].

In order to reproduce the scattering profiles, a model was introduced. Following Holy et al.[16], the scattering intensity stemming from a lateral periodic structure is given by

$$I(q_x, q_z) = \text{const.} \left|T_i T_f\right|^2 \left|C(q_x)\right|^2 \left|F(q_x, q_z)\right|^2$$

where $T_i$ and $T_f$ are the incident and exit transmission functions, which depend on the incident and exit angles and can give rise to multiple scattering for very thin films or multilayers (not the present film). In this case one might need to address the behavior of $T_i$ and $T_f$ with angle to understand the scattering data.

$$F(q_x, q_z) \equiv \int_0^\ell e^{-iq_z h(x) - iq_x x} dx$$

is the Fourier transform of the height profile function $h(x)$ of the surface, covering one terrace of each kind. In our case

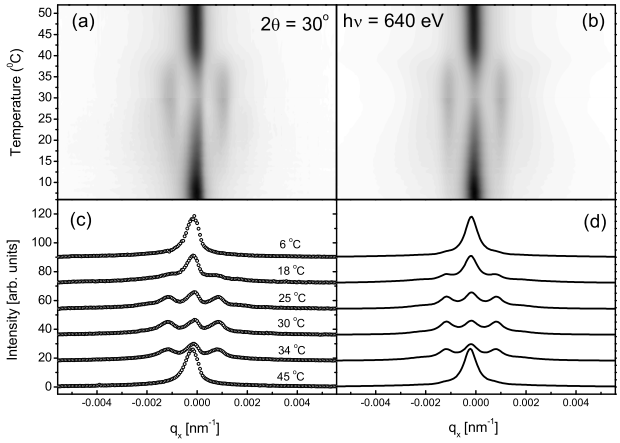


Figure 2: a) Two-dimensional plot of diffuse scattered intensity measured at $2\theta = 30^\circ$ as a function of $q_x$ (i.e. sample angle ω) and of temperature in the phase coexistence region and b) Corresponding fitted profiles following the model given in the text; c) Selected X-ray scans for different temperatures; d) Fitted profiles for corresponding scans on the left. Each profile was fitted separately according to equation 1.

$h(x)$ is given by

$$h(x) \equiv \begin{cases} 0, \text{ if } 0 < x < s \\ h_0, \text{ if } s < x < \ell \end{cases},$$

where $s$ is the width of the β phase terrace and $\ell$ the sum of the widths of the two terraces.

$$C(q_x) \equiv \langle \sum_{m,n} \exp\left[-i(R_m - R_n) q_x\right] \rangle$$

is the correlation function of different sets of two terraces averaged over the whole sample surface. This correlation function is proportional to a periodic sequence of δ-like functions[16] centered at reciprocal lattice positions at intervals $g = \frac{2\pi}{\ell}$, resulting in

$$C(q_x) = N \langle g \sum_{p=-\infty}^{\infty} \delta(q_x - pg) \rangle,$$

where N is the number of periods. These δ-like functions take a Lorentzian-like lineshape with full-width σ. This finite width here represents the combination of the limited coherence length of the x-ray beam and the correlation length of the stripes. We obtain the intensity profile, which in our was limited to the first 4 reciprocal lattice points

$$I(q_x, q_z) \propto \left|T_i T_f\right|^2 \left\{ \frac{s^2 + (\ell - s)^2 + 2\cos(q_z h)\,\ell(\ell - s)}{q_x^2 + \sigma^2} \right. \quad (1)$$

$$\left. + 16 \sin\left(\frac{hq_z}{2}\right) \sum_{p=-4(p\neq 0)}^{4} \frac{\frac{\sin\left(\frac{\pi p s}{\ell}\right)^2}{|p|^3 \left(\frac{2\pi}{\ell}\right)^2}}{\left(\frac{q_x}{p} - \frac{2\pi}{\ell}\right)^2 + \sigma^2} \right\}$$

In figures 2c and 2d the results of calculations are compared to the corresponding experimental results of 2a and 2b. The

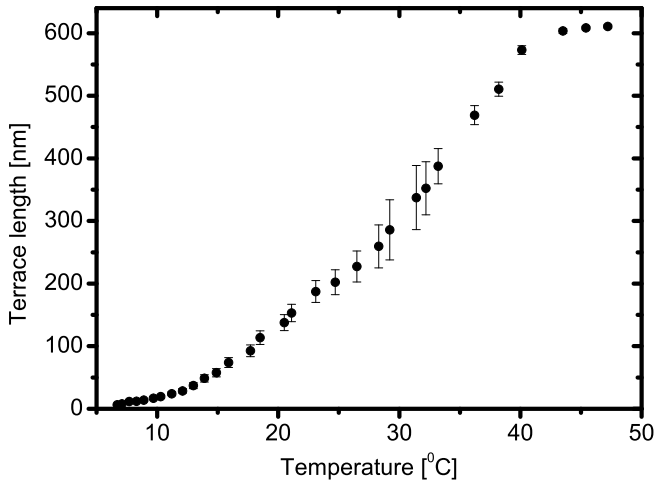


Figure 3: Temperature dependence of the β phase terrace width. The error bars are estimated from the statistical fluctuation of the scattered intensities of the specular and first diffuse satellite peaks. The error bars are larger in the intermediate temperature region due to the lower intensity of the specular peak.

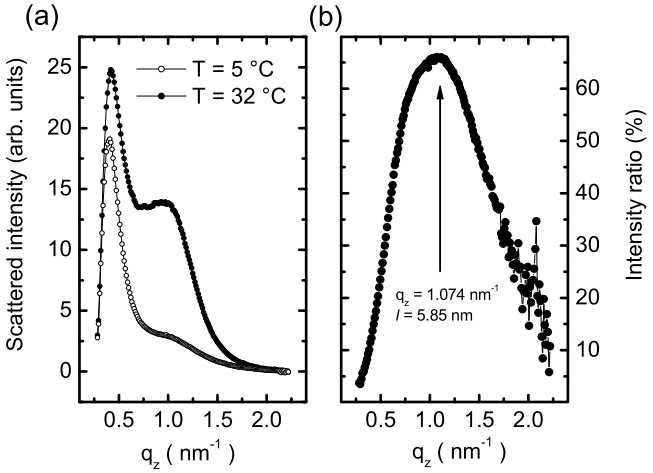


Figure 4: a) Scattered intensity as a function of vertical momentum transfer $q_z$ for a parallel momentum transfer $q_z$ for a parallel momentum transfer $q_x = 0.0107\,nm^{-1}$. Hollow circles: T = 5°C; filled circles: T = 32°C; b) Intensity ratio $\frac{I(T=320C)-I(T=50C)}{I(T=320C)+I(T=50C)}$ of the two curves in a), used to determine the terrace height.

intensity profiles were fitted separately for each temperature, using $s$, $\ell$ and σ and an overall scaling factor as fitting parameters. This model clearly reproduces extremely well the scattering data. The parameter $\sigma = (3.2 \pm 0.1) \times 10^{-4} nm^{-1}$ remained constant throughout all measurements, which indicates that the major source of broadening comes from the finite coherence length of the x-ray beam.

In order to evaluate the relative weight of the α and β phases, one can reduce the number of fitting parameters by limiting the analysis to the ratio between the intensities of the first order peak and of the specular reflectivity. In this case the intensity ratio of these two peaks as predicted by equation 1 is approximately given by[17]

$$\frac{I\left(q_x = \frac{2\pi}{\ell}\right)}{I\left(q_x = 0\right)} = \frac{16 \sin\left(\frac{hq_z}{2}\right) \sin\left(\frac{\pi s}{\ell}\right)^2 / \left(\frac{2\pi}{\ell}\right)^2}{s^2 + (\ell - s)^2 + 2\cos\left(q_z h\right) \ell\,(\ell - s)} \qquad (2)$$

The terrace width was determined by solving numerically equation 2 independently from other fitting parameters. As a result, much smaller error bars for the terrace width were obtained. Fig. 3 shows the temperature dependence of the β-phase terrace width.

Finally, we have measured the scattered intensity as a function of $q_z$ for a constant non-zero value of $q_x$. This can be obtained by independently positioning sample and detector angles according to a predetermined set of values. Fig. 4a shows the results of two $q_z$ scans ($T = 5°C$ and $T = 32°C$) taken at $q_x = 0.0107\,nm^{-1}$, i.e. at $q_x$ value matching the lateral order parameter of the stripes. Besides the peak of the transmission function (at $q_z = 0.4\,nm^{-1}$) present in scans perpendicular to the surface, at $T = 32°C$ there is a second peak centered around $q_z = 1\,nm^{-1}$, which comes from the interference between the waves scattered at the lower and the higher terraces.

In order to eliminate the contribution of the transmission function and to enhance the interference term, Fig. 4b shows the intensity ratio of the two scans. This ratio is centered at $q_z = 1.08 \pm 0.02\,nm^{-1}$, corresponding to a difference in height between the two stripes of $5.82\,nm$ (this height corresponds to an average value over the whole sample surface).

In contrast to the surface morphologic microscopy techniques, the X-ray technique used here probes wide area and the depth of the film including also the different X-ray absorption edges to select the structures involving particular atomic elements. This will allow the determination of chemical/magnetic ordering of specific atoms belonging to the crystal lattice. The introduction of this technique will therefore be useful in special cases where microscopy techniques are not appropriate.

It is also important to understand why such diffuse satellites were not previously observed in x-ray diffraction experiments[9,10]: there, one mainly observed Bragg peaks, which are sensitive to atomic distances of individual terraces. The radiation is scattered by atoms and variations in the terrace widths lead to an incoherent sum of the x-ray waves from neighboring terraces. In our present reflectivity method, one is not sensitive to the details of the crystal structure. The x-ray wave does not lose coherency when scattered by each terrace and the resulting interference pattern reveals the modulation of the surface structure.

In summary, we demonstrate in this work that the resonant soft X-ray diffuse reflectivity method is a powerful tool to investigate microscopic structures such as the terrace-like structures of MnAs/GaAs(001) films. We observed a clear long range periodic arrangement of stripe-like micro-structures alternating between α and β phases during the phase coexistence, which takes place between 10 and 45 °C. The period of the modulation structure obtained is about 600 nm, which remains constant with the temperature. The results are in good

agreements with those reported in similar MnAs films using different experimental techniques.

The authors thank the personnel of the LURE laboratory for technical support. R.M-P. and H.W.Jr. thank FAPESP, CNPq, FAPEMIG and Instituto do Milênio (Nanociências) for financial support.

[1] M. Tanaka, Semicond. Sci. Technol. 17, 327 (2002).
[2] M. Ramsteiner, R. H. Hao, A. Kawaharazuka, H. J. Zhu, M. Kästner, R. Hey, L. Däweritz, H. R. Grahn, and K. H. Ploog, Phys. Rev. 66, 81304 (2002).
[3] C. Guillard, J. Phys. Radium 12, 223 (1951).
[4] B. T. M. Willis and H. P. Rooksby, Proc. Phys. Soc. London, Sect. B 67, 290 (1954).
[5] N. Menyuk, J. A. Kafala, K. Dwinght, and J. B. Goodenough, Phys. Rev. 177, 942 (1969).
[6] M. Tanaka, J. P. Harbison, T. Sands, T. L. Cheeks, V. G. Keramides, and G. M. Rothberg, J. Vac. Sci. Technol. B 12, 1091 (1994).
[7] M. Tanaka, J. P. Harbison, M. C. Park, Y. S. Park, T. Shin, and G. M. Rothberg, Appl. Phys. Lett. 65, 1964 (1994).
[8] F. Schippan, A. Trampert, L. Däweritz, and K. H. Ploog, J. Vac. Sci. Technol. B 17, 1716 (1999).
[9] V.M. Kaganer, B. Jenichen, F. Schippan, W. Braun, L. Däweritz, and K.H. Ploog, Phys. Rev. Lett. 85, 341 (2000).
[10] V. M. Kaganer, B. Jenichen, F. Schippan, W. Braun, L. Däweritz, and K. H. Ploog, Phys. Rev. B 6, 45305 (2002).
[11] M. Kästner, C. Herman, L. Däweritz, and K. H. Ploog, J. Appl. Phys. 92, 5711 (2002).
[12] T. Plake, M. Ramsteiner, V. M. Kaganer, B. Jenichen, M. Kästner, L. Däweritz and K. H. Ploog, Appl. Phys. Lett. 80, 2523 (2002).
[13] F. Schippan, G. Behme, L. Däweritz, K. H. Ploog, B. Dennis, K.-U. Neumann, and K. R. A. Ziebeck, J. Appl. Phys. 88, 2766 (2000); T. Plake, T. Hesjedal, J. Mohanty, M. Kästner, L. Däweritz, and K. H. Ploog, Appl. Phys. Lett. 82, 2308 (2003); R. Engel-Herbert, J. Mohanty, A. Ney, T. Hesjedal, L. Däweritz, and K. H. Ploog, Appl. Phys. Lett. 84, 1133 (2004).
[14] E. Bauer, S. Cherifi, L. Däweritz, M. Kästner, S. Heun, and A. Locatelli, J. Vac. Sci. Technol. B 20, 2539 (2002)
[15] M.Sacchi, C.Spezzani, P.Torelli, A.Avila, R.Delaunay, and C.F.Hague, Rev. Sci. Instrum. 74, 2791 (2003).
[16] V. Holy, T. Roch, J. Stangl, A. Daniel, G. Bauer, T. H. Metzger, Y. H. Zhu, K. Brunner, and G. Abstreiter, Phys. Rev. B 63, 205318 (2001).
[17] In this procedure we have subtracted the contribution of the specular peak from the intensity of the first satelite peak, i.e., we have substracted the nearly temperature independent component of the intensity of the first satellite. In this case, $\frac{I(q_x=\frac{2\pi}{t})}{I(q_x=0)}$ is aproximatelly given by the ratio of the second (p = 1) and first terms of eq. 6, leading to eq. 7.